Heterogeneous & Homogeneous & Bio-

CHEMCATCHEM

CATALYSIS

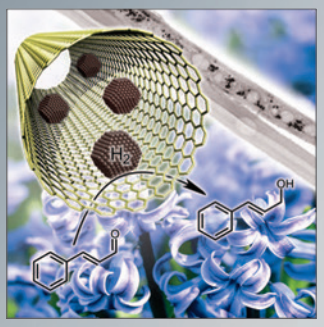

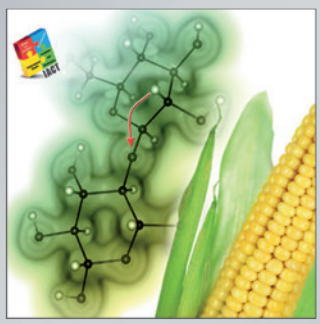

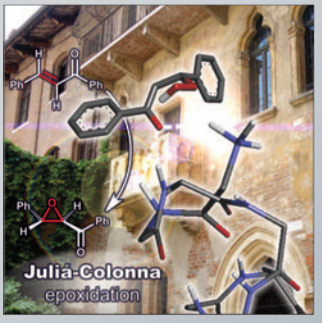

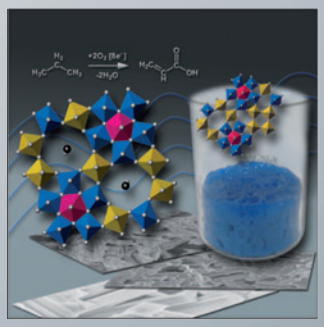

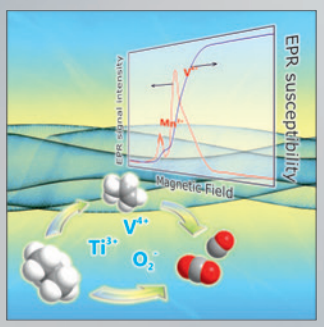

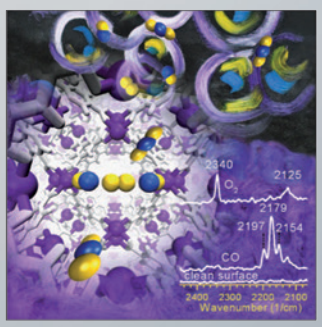

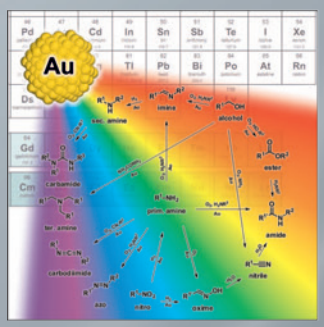

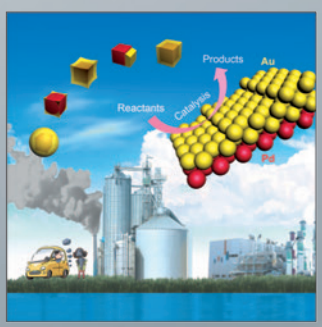

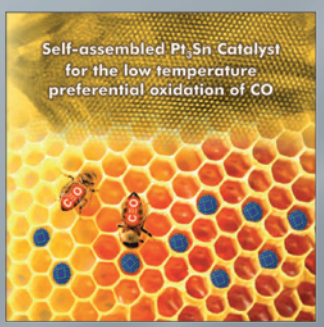

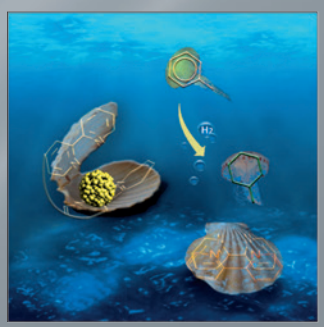

Reprint

A Journal of

ChemPubSoc Europe

WILEY-VCH

www.chemcatchem.org

ChemPubSoc Europe

DOI: 10.1002/cctc.201900987

CHEMCATCHEM Full Papers

Nitrogen Atoms as Stabilizers and Promoters for Ru-Cluster-Catalyzed Alkaline Water Splitting

Hao Hu[+],[a] Farhad M. D. Kazim[+],[a] Quan Zhang,[a] Konggang Qu,[b] Zehui Yang,*[a] and Weiwei Cai*[a]

Here, we report an efficient hydrogen evolution reaction (HER) and oxygen evolution reaction (OER) electrocatalyst, in which ruthenium clusters with a diameter of ~1 nm are anchored on nitrogen doped carbon (Ru/N-BP2000). Significantly low overpotentials are required for Ru/N-BP2000 to catalyze HER (15 mV vs. RHE) and OER (285 mV vs. RHE) in 1 M KOH with current density of 10 mA cm^{-2}, which outperforms Ru/BP2000 (HER: 54.2 mV vs. RHE; OER: 337 mV vs. RHE) as well as the benchmark Pt/C (52 mV vs. RHE) and IrO_2 (301 mV vs. RHE). Moreover, ignorable losses in electrocatalytic activities toward HER and OER are recorded for Ru/N-BP2000 electrocatalyst ascribed to the electronically delocalized Ru atoms induced by the nitrogen atoms. Only 1.53 V is needed for Ru/N-BP2000 electrocatalyst to drive overall water splitting with stable current density of 10 mA cm^{-2} for 50 h, which is comparably lower than Pt/C–IrO_2 demanding 1.59 V to attain 10 mA cm^{-2}. This work demonstrates the importance of nitrogen doping for promoting the Ru based electrocatalyst's activity and stability in water splitting application.

Introduction

Hydrogen, recognized as one of the most promising alternative energy sources to traditional fossil fuels, attracts much attention due to its high energy density, sustainability and zero-mission.[1] Hydrogen could be electrochemically generated from the water splitting driven by the intermittent power sources; however, the large-scale application of water splitting for massive H_2 generation is still limited due to the sluggish kinetics of the cathodic hydrogen evolution reaction (HER) and anodic oxygen evolution reaction (OER), which are uphill with high overpotentials resulting in high operational voltage than theoretical voltage (1.23 V) for water splitting, as a consequence, energy consumption is increased.[2] Platinum (Pt) and iridium oxides (IrO_2) are the state-of-the-art electrocatalysts for catalyzing HER and OER, respectively;[3] while, the high cost and limited reservation block the widespread application in industrial water splitting.[4] Thus, developments of cost-effective and highly active electrocatalysts for HER and OER are prominently important for water splitting technology.[5]

Until now, intensive investigations have been dedicated to the development of non-noble metal electrocatalysts as alternatives for Pt and IrO_2.[6] Especially, transitional metal oxides,[7] phosphides,[8] nitrides,[9] sulfides,[10] carbides[1b,11] and selenides[12] have been extensively researched as bifunctional electrocatalysts for HER and OER. However, these non-noble metal based electrocatalysts only exhibited comparable electrocatalytic activity toward HER or OER to Pt or IrO_2 electrocatalyst with high loading of electrocatalyst ascribed to the low intrinsic catalytic capability of HER or OER. Ruthenium (Ru) based electrocatalysts have been numerously reported since the price of Ru was 10 times lower than that of Pt and the intrinsic HER activity of Ru based electrocatalyst was comparable or superior to the benchmark Pt/C with similar or lower Ru dosage.[13] Surprisingly, these Ru based electrocatalysts have not been reported for OER catalysis in alkaline electrolyte yet, even RuO_2 perform an outstanding OER activity, which could be ascribed to the dissolution of the electrochemically generated ruthenium oxides (RuO_x, $x > 2$) in alkaline medium resulting in deterioration in water splitting performance.[14] Very recently, Sun *et al.* reported that Ru single atom (Ru-SA) anchored by cobalt-iron layered double hydroxides (Ru-SA/CoFe-LDHs) exhibited exceptional OER activity and stability due to the strong electronic coupling between CoFe-LDHs and Ru atoms.[15] Meanwhile, Chen *et al.* described that the lower electron density at Ru sites boosted the OER activity and stability of $Cr_{0.6}Ru_{0.4}O_2$ electrocatalyst in 0.5 M H_2SO_4 electrolyte.[16] Thus, the electronic delocalization could promote the OER activity and stability of Ru based electrocatalyst. Apart from the Ru, Xu *et al.* has reported that nitrogen atom could effectively anchor the Pt atoms and improved its stability and oxygen reduction reaction (ORR) activity.[17] Theoretically, Ru atoms also could be stabilized by nitrogen atoms due to the similar electronic structures to Pt and a promoted OER activity would be achieved since RuN_x species have been reported as facilitator for water dissociation process.[18] Besides, the incorporated nitrogen atoms were favorable for HER due to the additional active sites originating

[a] H. Hu,[+] F. M. D. Kazim,[+] Q. Zhang, Prof. Dr. Z. Yang, Prof. Dr. W. Cai
Sustainable Energy Laboratory
Faculty of Materials Science and Chemistry
China University of Geosciences Wuhan
388 Lumo RD
Wuhan 430074 (P. R. China)
E-mail: yeungzehui@gmail.com
willcai1985@gmail.com

[b] Prof. Dr. K. Qu
School of Chemistry and Chemical Engineering
Liaocheng University
Liaocheng 252059 (P. R. China)

[+] These authors equally contributed to this work.

Supporting information for this article is available on the WWW under https://doi.org/10.1002/cctc.201900987

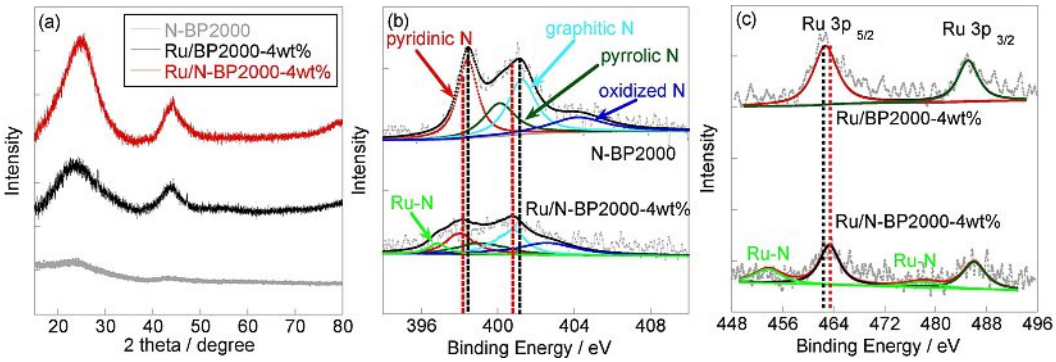

Figure 1. (a) XRD patterns of N-BP2000, Ru/BP2000-4 wt% and Ru/N-BP2000-4 wt% electrocatalysts. (b) Deconvoluted N1s peaks of N-BP2000 and Ru/N-BP2000-4 wt%. (c) Deconvoluted Ru3p peaks of Ru/BP2000-4 wt% and Ru/N-BP2000-4 wt%.

from the nitrogen doped carbon (NC). Thus, based on the above consideration, nitrogen atoms could boost the HER, OER activities and relative stability of Ru based electrocatalyst.

In order to prove the above-mentioned predication, here, we compared the HER and OER activities of Ru/BP2000 and Ru/N-BP2000 electrocatalysts synthesized via one-pot carbonization of BP-2000, urea and $RuCl_3$ as C, N and Ru sources, respectively. Due to the presence of nitrogen atoms in carbon framework, Ru/N-BP2000 exhibited better electrocatalytic activity for water splitting and excellent stability, which required only 1.53 V for achieving current density of 10 mA cm^{-2} and ignorable degradation was observed for 50 h.

Results and Discussion

Three electrocatalysts with different Ru contents (Ru/N-BP2000-2 wt%, Ru/N-BP2000-4 wt% and Ru/N-BP2000-8 wt%) and Ru/BP2000-4 wt% were synthesized. the XRD test was carried out to identify the crystal structure shown in Figure 1a, in which peaks at 25° and 43° assigned to the (002) facet of graphitic carbon and (101) facet of the metallic Ru (JCPDS: No. 01–1253) were observed for Ru/BP2000-4 wt% and Ru/N-BP2000-4 wt% electrocatalysts; meanwhile, similar peaks were observed for Ru/N-BP2000-2 wt% and Ru/N-BP2000-8 wt% (Figure S1) indicating a successful reduction of the Ru precursor. Diffraction peak at 25° was observed for N-BP2000 corresponding to (002) facet of graphitic carbon due to the high temperature (950 °C) during the synthesis of electrocatalyst. In order to know the electronic interaction between nitrogen and ruthenium atoms, XPS test was carried out and shown in Figure S2a. A new peak at 400 eV was observed for Ru/N-BP2000-2 wt%, Ru/N-BP2000-4 wt% and Ru/N-BP2000-8 wt% electrocatalysts ascribed to the N1s core level XPS spectrum originating from the decomposition of urea to generate NH_3 etching BP-2000 resulting in nitrogen doped carbon. The deconvoluted N1s peak of N-BP2000 depicted that oxidized N at 404.4 eV, graphitic N at 401.3 eV, pyrrolic N at 400 eV and pyridinic N at 398.5 eV were the dominant N species in N-BP2000 (Figure 1b).[19] A negative shift (0.2 eV) was observed in N1s peak for Ru/N-BP2000-4 wt% with relative to N-BP2000 with the calibrated C1s peak centered at 284.5 eV (Figure S2b), which was due to the strong interaction between N and Ru atoms. During the synthesis, Ru species were stabilized by nitrogen atoms via Ru–N bond similar to Pt–N and electrons were transferred from 5 s orbital of Ru to N atoms leading to the positively charged Ru atoms proved by the Ru–N bond observed at 397.5 eV in the deconvoluted N1s peak of Ru/N-BP2000-4 wt% electrocatalyst;[20] as a consequence, Ru3p peak of Ru/N-BP2000-4 wt% was positively shifted by 0.2 eV compared to that of Ru/BP2000-4 wt% (Figure 1c).[21] Ru/N-BP2000-2 wt% and Ru/N-BP2000-8 wt% electrocatalysts exhibited similar electronic structures to Ru/N-BP2000-4 wt% shown in Figure S(3–4). Besides, the XPS quantitative analysis suggested that all the electrocatalysts have similar nitrogen content as shown in Table S1. As shown in Figure 2a, Ru cluster was well dispersed on BP-2000 (Figure 2a) and N-BP2000 (Figure 2c) confirmed by the lattice spacing of 0.22 nm ascribed to the dominant (101) facet of Ru shown in Figure 2(b, d). HAADF-STEM image and related EDS mappings of Ru/N-BP2000-4 wt% depicted that N and Ru were well dispersed on BP-2000 (Figure 2e). Similarly, well dispersed Ru cluster on N-BP2000 were observed for Ru/N-BP2000-2 wt% (Figure S5) and Ru/N-BP2000-8 wt% (Figure S6) electrocatalysts. The diameters of Ru cluster were 1.2 ± 0.2 nm, 1.0 ± 0.1 nm, 1.1 ± 0.2 nm and 1.5 ± 0.1 nm for Ru/BP2000-4 wt %, Ru/N-BP2000-2 wt%, Ru/N-BP2000-4 wt% and Ru/N-BP2000-8 wt% electrocatalysts (Figure S7). The Ru loading on BP-2000 was confirmed to 1.8 wt%, 3.8 wt% and 8.2 wt% for Ru/BP2000-4 wt%, Ru/N-BP2000-2 wt%, Ru/N-BP2000-4 wt% and Ru/N-BP2000-8 wt% by TGA test shown in Figure S8, which was consistent with ICP-OES test. The Ru content was close to theoretical value indicating that Ru(III) species were almost completely reduced to metallic Ru.

Electrocatalytic activity toward hydrogen evolution reaction (HER) is conducted in N_2 purged 1 M KOH electrolyte. All LSV curves were iR compensated by solution resistance. Onsetpotentials (overpotential@1 mA cm^{-2}) of Ru/N-BP2000-4 wt% (4 mV vs. RHE, Figure 3a) and Ru/N-BP2000-8 wt% (3.8 mV vs. RHE, Figure S9) were lower compared to the benchmark Pt/C (10 mV vs. RHE), Ru/BP2000-4 wt% (11.4 mV vs. RHE) and Ru/N-

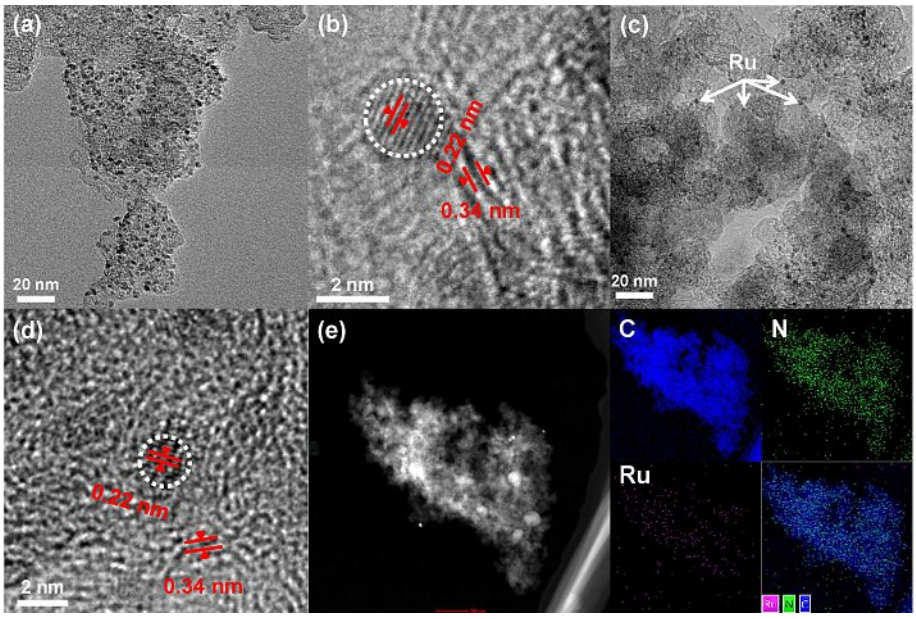

Figure 2. TEM and HR-TEM images of Ru/BP2000-4 wt% (a, b) and Ru/N-BP2000-4 wt% (c, d) electrocatalysts. (e) HAADF-STEM image and relative EDS mappings of Ru/N-BP2000-4 wt% electrocatalyst.

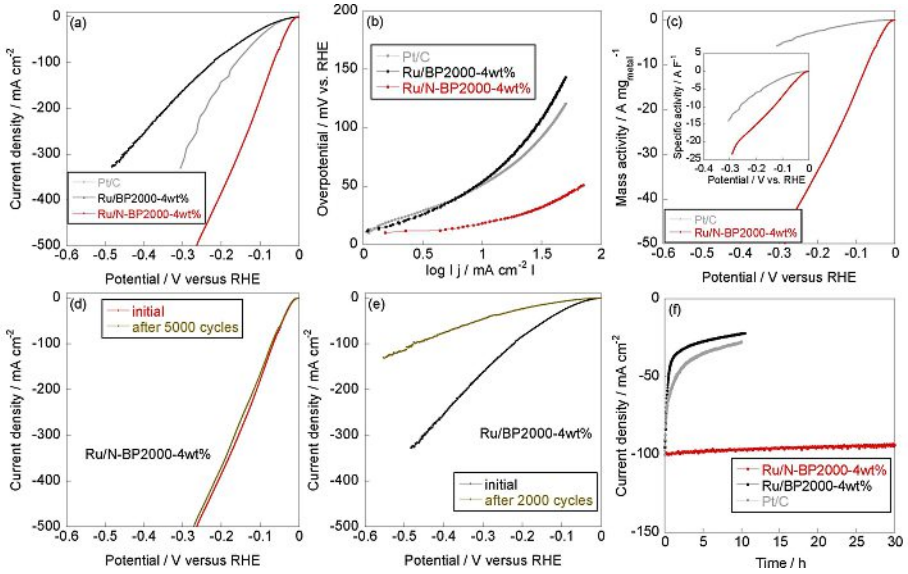

Figure 3. HER performance (a), Tafel slopes (b) of Pt/C, Ru/BP2000-4 wt% and Ru/N-BP2000-4 wt% electrocatalysts tested in 1 M KOH electrolyte. (c) Mass activities of commercial Pt/C and Ru/N-BP2000-4 wt% electrocatalysts; specific activities of commercial Pt/C and Ru/N-BP2000-4 wt% electrocatalysts were inserted. Durability results of Ru/N-BP2000-4 wt% (d) and Ru/BP2000-4 wt% (e) tested in 1 M KOH electrolyte. (f) Chronoamperometric stability test of Pt/C, Ru/BP2000-4 wt% and Ru/N-BP2000-4 wt% electrocatalyst at different overpotentials for attaining 100 mA cm^{-2}.

BP2000-2 wt% (16.1 mV vs. RHE). The lower required onsetpotential for Ru/N-BP2000-4 wt% electrocatalyst compared to Ru/BP2000-4 wt% was due to the lower energy barrier for Ru catalyzing water dissociation by the introduction of nitrogen atoms ($*+H_2O+e^-\rightarrow *H_{ads}+OH^-$,* represents the active site), which was the Volmer reaction of HER in alkaline medium.[22] Ru/N-BP2000-4 wt% (15 mV vs. RHE, Figure 3a) and Ru/N-BP2000-8 wt% (20 mV vs. RHE, Figure S9) required lower overpotentials to achieve catalytic current density of 10 mA cm^{-2} compared to the Ru/N-BP2000-2 wt%, Ru/BP2000-4 wt% and Pt/C electrocatalysts needing overpotentials of 63.5 mV, 54.2 mV and 46 mV vs. RHE to attain 10 mA cm^{-2}; moreover, only 150 mV overpotential was required for Ru/N-BP2000-4 wt% to achieve current density of 300 mA cm^{-2}, which was much lower compared to the Ru/N-BP2000-8 wt% (440 mV vs. RHE) and Pt/C (295 mV vs. RHE) indicating that Ru/N-BP2000-4 wt% possessed the best electrocatalytic activity toward HER. Ru/N-BP2000-4 wt% was recognized as one of the most efficient Ru-

based HER electrocatalysts as shown in Table S2. Compared to Ru/N-BP2000-8 wt% electrocatalyst, Ru/N-BP2000-4 wt% performed a better HER activity due to the smaller size of Ru cluster; thus, smaller size of Ru cluster and additional nitrogen atoms in Ru/N-BP2000-4 wt% co-contributed to its superior HER activity. The highest HER activity of Ru/N-BP2000-4 wt% was ascribed to the largest ECSA (25.5 mF cm^{-2}) estimated from double layer capacitance compared to commercial Pt/C (23.6 mF cm^{-2}), Ru/BP2000-4 wt% (16.4 mF cm^{-2}), Ru/N-BP2000-2 wt% (21.0 mF cm^{-2}) and Ru/N-BP2000-8 wt% (24.6 mF cm^{-2}) electrocatalysts as shown in Figure S10. Due to the introduction of nitrogen atoms to the electrocatalyst, the nitrogen nearby Ru cluster could also adsorb hydrogen ions and facilitate the recombination of hydrogen atoms to release H_2 molecule contributing to a boosted HER activity of Ru/N-BP2000-4 wt% compared to Ru/BP2000-4 wt% electrocatalyst proved by the higher HER performance of N-BP2000 than BP-2000 shown in Figure S11. Charge transfer resistance (R_{ct}) is another essential parameter to evaluate the HER activity. As shown in Figure S12a, R_{ct} of Ru/N-BP2000-4 wt% was 26 Ω, which was comparably lower than those of Ru/BP2000-4 wt% (70 Ω), Ru/N-BP2000-2 wt% (72 Ω) and Ru/N-BP2000-8 wt% (48 Ω) indicating an efficient electron transfer during the HER test. In order to study the kinetics of HER, the Tafel slope was calculated and shown in Figure S3b, in which Tafel slopes were 54.7 mV dec^{-1}, 84.5 mV dec^{-1}, 86.2 mV dec^{-1}, 30.4 mV dec^{-1} and 39.9 mV dec^{-1} for commercial Pt/C, Ru/BP2000-4 wt%, Ru/N-BP2000-2 wt%, Ru/N-BP2000-4 wt% and Ru/N-BP2000-8 wt% suggesting that all the electrocatalysts followed Volmer-Heyrovsky mechanism, in which Heyrovsky step ($H_2O + {}^*H_{ads} + e^- \rightarrow H_2 + OH^- + {}^*$) is the rate-limiting step during the HER.[23] The lowest Tafel slope of Ru/N-BP2000-4 wt% elucidated that more actives sites were involved in Heyrovsky step.[24] In order to make a fair comparison, the mass/specific activity was shown in Figure 3c and Ru/N-BP2000-4 wt% exhibited a better intrinsic electrocatalytic activity toward HER due to the small Ru size triggering high utilization efficiency. Meanwhile, Faradaic efficiency of Ru/N-BP2000-4 wt% was calculated to 100% as shown in Figure S13. The durability is another important parameter to evaluate the HER electrocatalyst. As shown in Figure 3d, ignorable degradation in HER performance (only 8 mV shift at 500 mA cm^{-2}) was recorded for Ru/N-BP2000-4 wt% electrocatalyst after 5000 potential cycles ascribed to the high similarity in ECSA (24.2 mF cm^{-2}) calculated from the double layer capacitances after durability test and slightly increased R_{ct} from 26 Ω to 27 Ω (Figure S14). In contrast, Ru/BP2000-4 wt% exhibited a serious deterioration in HER performance (Figure 3e) due to the sharp loss in ECSA (from 21.2 mF cm^{-2} to 7.2 mF cm^{-2} after 2000 potential cycles) as well as the significantly increased R_{ct} (Figure S15) due to the weak interaction between Ru atoms and BP-2000; in contrast, the nitrogen heteroatoms doping could boost the interaction between Ru and nitrogen atoms resulting in higher durability proved by the HAADF-STEM image and related EDS mappings after durability test (Figure S16). And the lattice spacing of 0.22 nm was confirmed to the dominant (101) facet of Ru, which was consistent with the XRD test (Figure S17) having a diffraction peak centered at 43 °C corresponding to the Ru(101). The benchmark Pt/C also faced a serious degradation in HER electrocatalytic activity after 2000 potential cycles with overpotential@10 mA cm^{-2} increased from 46 mV to 83 mV vs. RHE attributed to the decrement in ECSA (**Figure S18**) because of the high mobility of Pt nanoparticles on carbon black. Consequently, the chronoamperometric stability of Ru/N-BP2000-4 wt% electrocatalyst was tested with applied voltage of −66 mV vs. RHE to delivering cathodic current density of 100 mA cm^{-2} in order to simulate the practical condition of water splitting. As shown in Figure 3f, the current density was maintained at 100 mA cm^{-2} for 30 h highlighting the exceptional stability of the fabricated Ru/N-BP2000-4 wt% electrocatalyst; in contrast, current densities of Ru/BP2000-4 wt% and commercial Pt/C were dramatically decreased to 50 mA cm^{-2} after only 0.5 h and to 10 mA cm^{-2} after 10 h catalysis. The chronoamperometric stability test also emphasized the importance of nitrogen atoms for the promotion in stability.

As well known, metal nanoparticles could be electrochemically oxidized to metal oxides or hydroxides under high voltage.[8a,25] Ru atoms could be transferred to Ru oxides (RuO_x) and a high OER activity of Ru/N-BP2000-4 wt% was predictable; thus, the oxygen evolution reaction (OER) of Ru/N-BP2000-4 wt% was tested in O_2 purged 1 M KOH electrolyte. As shown in Figure 4a, overpotential for delivering 10 mA cm^{-2} was 285 mV vs. RHE for Ru/N-BP2000-4 wt%, which was lower compared to Ru/BP2000-4 wt% (337 mV vs. RHE) and benchmark IrO_2 (301 mV vs. RHE) electrocatalyst ascribed to the higher ECSA (Ru/N-BP2000-4 wt%: 8.5 mF cm^{-2}; Ru/BP2000-4 wt%: 4.2 mF cm^{-2}; IrO_2: 3.7 mF cm^{-2}) calculated from the double layer capacitances (Figure S19) as well as lower charge transfer resistance (Ru/N-BP2000-4 wt%: 95 Ω; Ru/BP2000-4 wt%: 132 Ω, Figure S20a). The improved OER activity of Ru/N-BP2000-4 wt% compared to Ru/BP2000-4 wt% was attributed to the additional nitrogen atoms in the electrocatalyst since the nitrogen doping induced ionized Ru atoms could be efficiently transferred to RuO_x as active sites for OER catalysis.[26] Tafel slopes, representing the kinetics of OER, were 70 mV dec^{-1} for Ru/N-BP2000-4 wt% (Figure S20b), which was lower than those of Ru/BP2000-4 wt% (123 mV dec^{-1}) and comparable to commercial IrO_2 (64 mV dec^{-1}) indicating that a faster discharge process of absorbed OH^- species on nitrogen anchored Ru atoms than pure Ru atoms.[27] Also, the durability test was conducted and Ru/N-BP2000-4 wt% electrocatalyst exhibited ignorable degradation in overpotential for delivering 10 mA cm^{-2} and 40 mA cm^{-2} (Figure 4b) due to the well-maintained ECSA (7.9 mF cm^{-2} after durability test) estimated from the double layer capacitances (Figure S21). Moreover, a similar R_{ct} was obtained before and after durability test shown in Figure S21c; while, electrocatalytic activity toward OER catalysis of Ru/BP2000-4 wt% was sharply decreased after 1000 potential cycles as shown in Figure 4c due to the decreased ECSA (2 mF cm^{-2} after durability test, Figure S22). In order to identify the higher durability of Ru/N-BP2000-4 wt% electrocatalyst, XPS was carried out and N1s and Ru3p peaks were still observed in Ru/N-BP2000-4 wt% electrocatalyst; while, in case of Ru/BP2000-4 wt%, Ru 3p peak was vanished due to the electrochemical

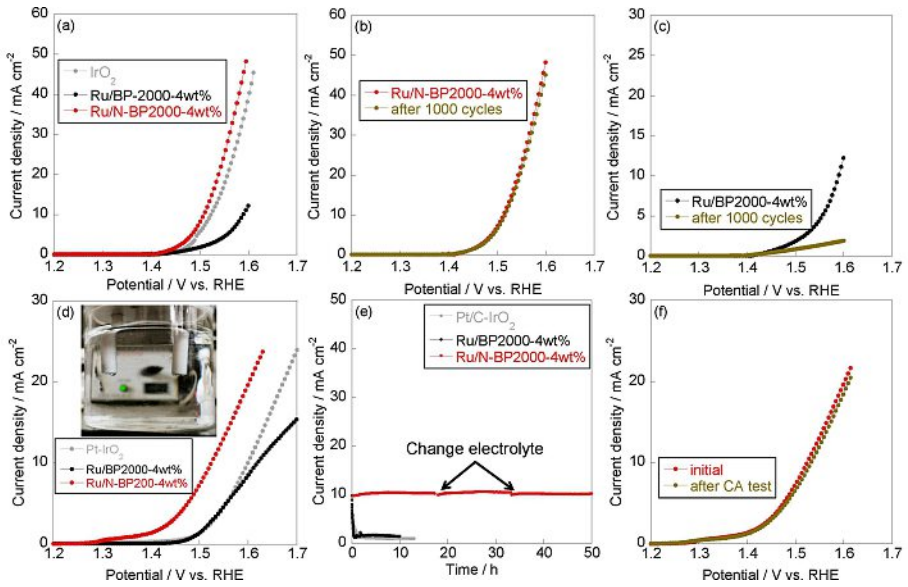

Figure 4. OER performances (a) of Ru/BP2000-4 wt%, Ru/N-BP2000-4 wt% and commercial IrO_2 electrocatalysts tested in O_2-purged 1 M KOH electrolyte. Durability results of Ru/N-BP2000-4 wt% (b) and Ru/BP2000-4 wt% (c) tested in O_2-purged 1 M KOH electrolyte. (d) LSV curves of water splitting driven by Pt-IrO_2, Ru/BP2000-4 wt% and Ru/N-BP2000-4 wt% electrocatalysts. (e) Chronoamperometric stability test of Pt/C–IrO_2, Ru/BP2000-4 wt% and Ru/N-BP2000-4 wt % electrocatalysts at different potentials for attaining 10 mA cm^{-2}. (f) LSV curves of water splitting driven by Ru/N-BP2000-4 wt% before and after CA test.

conversion of metallic Ru to RuO_2 (Ru^{4+}), which was dissolvable in alkaline medium (Figure S23). For Ru/N-BP2000-4 wt% electrocatalyst, Ru atoms were also converted to Ru oxides (Ru^{x+}, $x < 4$), which could be due to the formation of N–Ru-O bond. As reported previously, Ru oxides were electrochemically stable if low valence state (<4) of Ru was formed.[15] The quantitative analysis of XPS suggested that the weight ratio between N and Ru was almost stable during OER durability test (Table S1). Additionally, the durability test of benchmark IrO_2 was also studied as shown in Figure S24, in which a poor durability was recorded for IrO_2 and overpotential for delivering 10 mA cm^{-2} was increased by 174 mV after merely 1000 potential cycles.

Due to the high electrocatalytic activities toward HER and OER, for proof of concept, water splitting device was assembled by Ru/N-BP2000-4 wt% electrocatalyst and Pt/C–IrO_2 (Ru/BP2000-4 wt%) was utilized as control experiment. As shown in Figure 4d, 1.53 V was required to attain water splitting current density of 10 mA cm^{-2}, which was comparably lower than Pt–IrO_2 and Ru/N-BP2000-4 wt% demanding 1.59 V and 1.62 V. Due to the high stability, Ru/N-BP2000-4 wt% produced a stable current density of 10 mA cm^{-2} for 50 h; in contrast, current density was decreased to 1 mA cm^{-2} after 2 h for Pt/C–IrO_2 and Ru/BP2000-4 wt% due to the low stability of IrO_2 and Ru/BP2000-4 wt% under high potential (Figure 4e); additionally, Ru/N-BP2000-4 wt% performance similar water splitting performance after 50 h catalysis (Figure 4f) highlighting the exceptional stability. Thus, Ru/N-BP2000-4 wt% could potentially use as efficient electrocatalyst toward alkaline water splitting.

Conclusions

In summary, a 1 nm Ru cluster was anchored on nitrogen doped carbon (Ru/N-BP2000) via one-pot pyrolysis of BP-2000, urea and $RuCl_3$ at 950 °C. Ru/N-BP2000 exhibited good HER and OER activities with overpotentials of 15 mV and 285 mV vs. RHE to reach 10 mA cm^{-2} compared to Ru/BP2000 (HER: 54.2 mV vs. RHE; OER: 337 mV vs. RHE). Moreover, Ru/N-BP2000 exhibited negligible degradations in HER and OER activities after durability test; in contrast, sharp deterioration in electrocatalytic activity was recorded for Ru/BP2000. The boosted electrocatalytic activity and stability was attributed to the nitrogen atoms attracting electrons from 5 s orbitals of Ru atoms resulting in electronic delocalization of Ru. 1.53 V was required for Ru/N-BP2000 electrocatalyst to attain water splitting current density of 10 mA cm^{-2} comparably lower than benchmarking Pt/C–IrO_2 (1.59 V).

Experimental Section

Materials: The carbon black BP2000 was purchased from Asian-Pacific Specialty Chemicals Kuala Lumpur. Ruthenium(III) chloride ($RuCl_3$, $\geq$37.0 %) was purchased from Shanxi Kaida Chemical Engineering Co., Ltd. Nitric acid (HNO_3), potassium hydroxide (KOH, $>$85.0 %) and urea ($(NH_2)_2CO$, $>$99.0 %) were obtained from Sinopharm Chemical Reagent Co., Ltd. Nafion solution (5 wt%) and commercial Pt/C (Pt amount: 20 wt%) was obtained from Alfa Aesar. All the chemicals were used as received without any purification.

Synthesis of electrocatalyst: 100 mg of BP-2000 and 5.2 mg of ruthenium (III) chloride were dispersed in 30 mL of 6 M HNO_3 by stirring under 80 °C in an oil bath for 6 h. The resulting suspension was dried at 55 °C and then grounded together with 1.0 g urea. Ru/

N-BP2000 was synthesized from the pyrolysis of the mixed power at 950 °C for 1 h under argon atmosphere with heating rate of 5 °C min^{-1}. The samples synthesized by using different amounts of $RuCl_3$ were denoted as Ru/N-BP2000-2 wt%, Ru/N-BP2000-4 wt%, and Ru/N-BP2000-8 wt%, respectively. For comparison, a pure nitrogen-doped carbon (denoted as N-BP2000) and a pure carbon-supported ruthenium (denoted as Ru/BP2000) were also prepared in a similar way.

Material characterization: The crystal phase of synthesized powder was detected by X-ray diffraction (XRD, Bruker AXS D8-Focus, Germany) with Cu Kα radiation in the range of 2θ from 10° to 80°. The X-ray photoelectron spectroscopy (XPS) spectra were measured using Thermo-Scientific K-Alpha equipment. The TEM images were measured using a JEM-2010 electron microscope with voltage of 120 KV. The amount of ruthenium in the catalyst was calculated by the ICP-OES method using Perkin Elmer Optima 5300 DV.

Electrochemical measurements: All the electrochemical tests were conducted using Gamry (interface 1000E, USA) instrument with a typical three-electrode system. Hg/HgO electrode saturated with 1 M KOH solution and carbon rod were used as the reference and counter electrodes, respectively. 2 mg electrocatalysts were dispersed in 800 μL of deionized water, 185 μL of isopropanol and 15 μL of Nafion solution (5 wt%) by ultrasonic treatment for 0.5 h to obtain the homogeneous suspension. 10 μL of the resultant suspension was casted on a GCE (mass loading 0.285 mg cm^2) with a diameter of 3 mm and then dried. For HER test, LSV curve was recorded with a scan rate of 5 mV s^{-1} in N_2-saturated 1 M KOH solution. CV was carried out with 50 mV s^{-1} ranging from 0 to 1.2 V versus RHE. The electrochemical double-layer capacitance was measured from 0.16 V to 0.26 V vs. RHE with different scan rates from 10 to 100 mV s^{-1}. And ECSA value was obtained from the slope of scan rate versus capacitive current density@ 0.2 V vs. RHE. EIS was measured from 100 kHz to 0.05 Hz under AC voltage amplitude of 5 mV and DC voltage based at a given potential at 10 mA cm^{-2}. The long-term stability was measured by chronoamperometric (I-t) stability examination at given potential. Oxygen evolution reaction (OER) test was also carried out in O_2-saturated 1 M KOH solution. Water splitting test was performed in 1 M KOH solution using two electrodes with catalyst loading of 0.285 mg cm^2.

Acknowledgements

This work is supported by the National Natural Science Foundation of China (No. 21703212, 21875224) and Fundamental Research Funds for the Central Universities, China University of Geosciences (Wuhan) (CUG170615).

Conflict of Interest

The authors declare no conflict of interest.

Keywords: Hydrogen evolution reaction · Oxygen evolution reaction · Ruthenium · Nitrogen doped carbon · water splitting

[1] a) F. Luo, Q. Zhang, X. Yu, S. Xiao, Y. Ling, H. Hu, L. Guo, Z. Yang, L. Huang, W. Cai, H. Cheng, *Angew. Chem. Int. Ed.* **2018**, *57*, 14862–14867; b) C. Lu, D. Tranca, J. Zhang, F. N. Rodríguez Hernández, Y. Su, X. Zhuang, F. Zhang, G. Seifert, X. Feng, *ACS Nano* **2017**, *11*, 3933–3942; c) Y. P. Zhu, T. Y. Ma, M. Jaroniec, S. Z. Qiao, *Angew. Chem. Int. Ed.* **2017**, *56*, 1324–1328; *Angew. Chem.* **2017**, *129*, 1344–1348; d) K. Karthick, S. Anantharaj, S. Kundu, *ACS Sustainable Chem. Eng.* **2018**, *6*, 6802–6810; e) S. Anantharaj, M. Jayachandran, S. Kundu, *Chem. Sci.* **2016**, *7*, 3188–3205; f) N. Zhang, L. Cao, L. Feng, J. Huang, K. Kajiyoshi, C. Li, Q. Liu, D. Yang, J. He, *Nanoscale* **2019**, *11*, 11542–11549.

[2] a) C. Panda, P. W. Menezes, C. Walter, S. Yao, M. E. Miehlich, V. Gutkin, K. Meyer, M. Driess, *Angew. Chem. Int. Ed.* **2017**, *56*, 10506–10510; *Angew. Chem.* **2017**, *129*, 10642–10646; b) H. Li, S. Chen, Y. Zhang, Q. Zhang, X. Jia, Q. Zhang, L. Gu, X. Sun, L. Song, X. Wang, *Nat. Commun.* **2018**, *9*, 2452; c) Y. Liu, Q. Li, R. Si, G.-D. Li, W. Li, D.-P. Liu, D. Wang, L. Sun, Y. Zhang, X. Zou, *Adv. Mater.* **2017**, *29*, 1606200.

[3] Y. Liang, Y. Li, H. Wang, H. Dai, *J. Am. Chem. Soc.* **2013**, *135*, 2013–2036.

[4] a) F. Yu, H. Zhou, Y. Huang, J. Sun, F. Qin, J. Bao, W. A. Goddard, S. Chen, Z. Ren, *Nat. Commun.* **2018**, *9*, 2551; b) W. Lu, T. Liu, L. Xie, C. Tang, D. Liu, S. Hao, F. Qu, G. Du, Y. Ma, A. M. Asiri, X. Sun, *Small* **2017**, *13*, n/a-n/a.

[5] Z. Liu, Z. Zhao, Y. Wang, S. Dou, D. Yan, D. Liu, Z. Xia, S. Wang, *Adv. Mater.* **2017**, *29*, 1606207.

[6] S. Anantharaj, S. R. Ede, K. Sakthikumar, K. Karthick, S. Mishra, S. Kundu, *ACS Catal.* **2016**, *6*, 8069–8097.

[7] a) Y. Ji, L. Yang, X. Ren, G. Cui, X. Xiong, X. Sun, *ACS Sustainable Chem. Eng.* **2018**, *6*, 9555–9559; b) X. Yan, L. Tian, S. Atkins, Y. Liu, J. Murowchick, X. Chen, *ACS Sustainable Chem. Eng.* **2016**, *4*, 3743–3749; c) Y. Zhao, C. Chang, F. Teng, Y. Zhao, G. Chen, R. Shi, G. I. N. Waterhouse, W. Huang, T. Zhang, *Adv. Energy Mater.* **2017**, *7*, 1700005.

[8] a) C. Du, L. Yang, F. Yang, G. Cheng, W. Luo, *ACS Catal.* **2017**, *7*, 4131–4137; b) X. Zhong-Hua, S. Hui, Y. Qiu-Ying, Z. Bing, W. Hong-Hui, L. Xin-Hao, C. Jie-Sheng, *Adv. Energy Mater.* **2017**, *7*, 1602355; c) L. Jiayuan, Y. Ming, Z. Xuemei, H. Zheng-Qing, X. Zhaoming, C. Chun-Ran, M. Yuanyuan, Q. Yongquan, *Adv. Funct. Mater.* **2016**, *26*, 6785–6796.

[9] a) J. Hou, Y. Sun, Z. Li, B. Zhang, S. Cao, Y. Wu, Z. Gao, L. Sun, *Adv. Funct. Mater. 0*, 1803278; b) Z. Chen, Y. Ha, Y. Liu, H. Wang, H. Yang, H. Xu, Y. Li, R. Wu, *ACS Appl. Mater. Interfaces* **2018**, *10*, 7134–7144.

[10] a) Y. Yang, K. Zhang, H. Lin, X. Li, H. C. Chan, L. Yang, Q. Gao, *ACS Catal.* **2017**, *7*, 2357–2366; b) Z. Jian, W. Tao, P. Darius, R. Bernd, D. Renhao, L. Shaohua, Z. Xiaodong, F. Xinliang, *Angew. Chem. Int. Ed.* **2016**, *55*, 6702–6707; *Angew. Chem.* **2016**, *128*, 6814–6819.

[11] a) G.-E. A. T. C. Dongkyu, O. Yiwei, K. Jun, D. Kazunari, T. Kazuhiro, *ChemSusChem* **2013**, *6*, 168–181; b) Z.-Y. Yu, Y. Duan, M.-R. Gao, C.-C. Lang, Y.-R. Zheng, S.-H. Yu, *Chem. Sci.* **2017**, *8*, 968–973.

[12] a) K. Li, J. Zhang, R. Wu, Y. Yu, B. Zhang, *Adv. Sci.* **2016**, *3*, 1500426; b) X. Xu, H. Liang, F. Ming, Z. Qi, Y. Xie, Z. Wang, *ACS Catal.* **2017**, *7*, 6394–6399.

[13] a) J. Mahmood, F. Li, S.-M. Jung, M. S. Okyay, I. Ahmad, S.-J. Kim, N. Park, H. Y. Jeong, J.-B. Baek, *Nat. Nanotechnol.* **2017**, *12*, 441; b) Y. Li, L. A. Zhang, Y. Qin, F. Chu, Y. Kong, Y. Tao, Y. Li, Y. Bu, D. Ding, M. Liu, *ACS Catal.* **2018**, *8*, 5714–5720; c) B. Lu, L. Guo, F. Wu, Y. Peng, J. E. Lu, T. J. Smart, N. Wang, Y. Z. Finfrock, D. Morris, P. Zhang, N. Li, P. Gao, Y. Ping, S. Chen, *Nat. Commun.* **2019**, *10*, 631; d) S. Ji, Y. Chen, S. Zhao, W. Chen, L. Shi, Y. Wang, J. Dong, Z. Li, F. Li, C. Chen, Q. Peng, J. Li, D. Wang, Y. Li, *Angew. Chem. Int. Ed.*; e) J. Zhang, P. Liu, G. Wang, P. P. Zhang, X. D. Zhuang, M. W. Chen, I. M. Weidinger, X. L. Feng, *J. Mater. Chem. A* **2017**, *5*, 25314–25318; f) P. Zonghua, A. I. Saana, K. Zongkui, L. Wenqiang, M. Shichun, *Angew. Chem. Int. Ed.* **2017**, *56*, 11559–11564; *Angew. Chem.* **2017**, *129*, 11717–11722; g) J. Wang, Z. Wei, S. Mao, H. Li, Y. Wang, *Energy Environ. Sci.* **2018**, *11*, 800–806; h) X. Cheng, H. Wang, M. Ming, W. Luo, Y. Wang, Y. Yang, Y. Zhang, D. Gao, J. Bi, G. Fan, *ACS Sustainable Chem. Eng.* **2018**, *6*, 11487–11492; i) T. Qiu, Z. Liang, W. Guo, S. Gao, C. Qu, H. Tabassum, H. Zhang, B. Zhu, R. Zou, Y. Shao-Horn, *Nano Energy* **2019**, *58*, 1–10; j) H. Wang, C. Xu, Q. Chen, M. Ming, Y. Wang, T. Sun, Y. Zhang, D. Gao, J. Bi, G. Fan, *ACS Sustainable Chem. Eng.* **2019**, *7*, 1178–1184; k) Y. Wang, Z. Liu, H. Liu, N.-T. Suen, X. Yu, L. Feng, *ChemSusChem* **2018**, *11*, 2724–2729.

[14] a) T. P. Luxton, M. J. Eick, K. G. Scheckel, *J. Colloid Interface Sci.* **2011**, *359*, 30–39; b) S. Cherevko, S. Geiger, O. Kasian, N. Kulyk, J.-P. Grote, A. Savan, B. R. Shrestha, S. Merzlikin, B. Breitbach, A. Ludwig, K. J. J. Mayrhofer, *Catal. Today* **2016**, *262*, 170–180.

[15] P. Li, M. Wang, X. Duan, L. Zheng, X. Cheng, Y. Zhang, Y. Kuang, Y. Li, Q. Ma, Z. Feng, W. Liu, X. Sun, *Nat. Commun.* **2019**, *10*, 1711.

[16] Y. Lin, Z. Tian, L. Zhang, J. Ma, Z. Jiang, B. J. Deibert, R. Ge, L. Chen, *Nat. Commun.* **2019**, *10*, 162.

[17] J. Liu, M. Jiao, L. Lu, H. M. Barkholtz, Y. Li, Y. Wang, L. Jiang, Z. Wu, D.-j. Liu, L. Zhuang, C. Ma, J. Zeng, B. Zhang, D. Su, P. Song, W. Xing, W. Xu, Y. Wang, Z. Jiang, G. Sun, *Nat. Commun.* **2017**, *8*, 15938.
[18] a) N. D. Morris, M. Suzuki, T. E. Mallouk, *J. Phys. Chem. A* **2004**, *108*, 9115–9119; b) L. Duan, F. Bozoglian, S. Mandal, B. Stewart, T. Privalov, A. Llobet, L. Sun, *Nat. Chem.* **2012**, *4*, 418.
[19] H. Hu, Q. Zhang, F. Luo, L. Guo, K. Qu, Z. Yang, S. Xiao, Z. Xu, W. Cai, H. Cheng, *ChemElectroChem* **2019**, *6*, 1413–1418.
[20] S. Chen, Z. Wei, X. Qi, L. Dong, Y. G. Guo, L. Wan, Z. Shao, L. Li, *J. Am. Chem. Soc.* **2012**, *134*, 13252–13255.
[21] a) R. Vinoth, S. G. Babu, V. Bharti, V. Gupta, M. Navaneethan, S. V. Bhat, C. Muthamizhchelvan, P. C. Ramamurthy, C. Sharma, D. K. Aswal, Y. Hayakawa, B. Neppolian, *Sci. Rep.* **2017**, *7*, 43133; b) X. Zeng, C. You, L. Leng, D. Dang, X. Qiao, X. Li, Y. Li, S. Liao, R. R. Adzic, *J. Mater. Chem. A* **2015**, *3*, 11224–11231.
[22] Q. Zhang, Z. Yang, J. Yang, X. Yu, Y. Ling, Y. Zhang, W. Cai, H. Cheng, *Chem. Commun.* **2018**, *54*, 9282–9285.
[23] Y. Ling, Z. Yang, Q. Zhang, Y. Zhang, W. Cai, H. Cheng, *Chem. Commun.* **2018**, *54*, 2631–2634.
[24] Y. Li, H. Wang, L. Xie, Y. Liang, G. Hong, H. Dai, *J. Am. Chem. Soc.* **2011**, *133*, 7296–7299.
[25] X. Zhang, X. Zhang, H. Xu, Z. Wu, H. Wang, Y. Liang, *Adv. Funct. Mater.* **2017**, *27*, 1606635.
[26] a) X. Wang, A. Vasileff, Y. Jiao, Y. Zheng, S.-Z. Qiao, *Adv. Mater.*, 1803625; b) Q. Wang, Y. Ji, Y. Lei, Y. Wang, Y. Wang, Y. Li, S. Wang, *ACS Energy Lett.* **2018**, *3*, 1183–1191; c) C. Tang, H.-F. Wang, X. Chen, B.-Q. Li, T.-Z. Hou, B. Zhang, Q. Zhang, M.-M. Titirici, F. Wei, *Adv. Mater.* **2016**, *28*, 6845–6851; d) M. Li, L. Zhang, Q. Xu, J. Niu, Z. Xia, *J. Catal.* **2014**, *314*, 66–72.
[27] Y. Yang, D. Lianna, S. M. J., S. Hongyuan, L. Wenjie, C. Jie, X. Peng, Z. Yunhuai, H. R. J., J. Song, *Adv. Energy Mater.* **2018**, *8*, 1703189.

Manuscript received: May 31, 2019
Revised manuscript received: June 28, 2019
Accepted manuscript online: July 3, 2019
Version of record online: July 23, 2019